metals

MDPI

Article

Preparation of Two Novel Stable Silica-Based Adsorbents for Selective Separation of Sr from Concentrated Nitric Acid Solution

Chang Liu [1], Shichang Zhang [2], Xinpeng Wang [1,*], Lifeng Chen [3], Xiangbiao Yin [3], Mohammed F. Hamza [3], Yuezhou Wei [3,4] and Shunyan Ning [3,*]

[1] State Key Laboratory of Featured Metal Materials and Life-Cycle Safety for Composite Structures, MOE Key Laboratory of New Processing Technology for Nonferrous Metals and Materials, School of Resources, Environment and Materials, Guangxi University, Nanning 530004, China; liuchangguangxiedu@st.gxu.edu.cn

[2] School of Nuclear Science and Technology, University of Science and Technology of China, Hefei 230026, China; zhangshichang@mail.ustc.edu.cn

[3] School of Nuclear Science and Technology, University of South China, 28 Changsheng West Road, Hengyang 421001, China; chenlf@usc.edu.cn (L.C.); yinxb@usc.edu.cn (X.Y.); m_fouda21@usc.edu.cn (M.F.H.); yzwei@usc.edu.cn (Y.W.)

[4] School of Nuclear Science and Engineering, Shanghai Jiao Tong University, Shanghai 200240, China

* Correspondence: wangxinpeng@gxu.edu.cn (X.W.); ningshunyan@usc.edu.cn (S.N.); Tel.: +86-0771-3392507 (X.W.)

Abstract: Crown ethers are famous for the highly selectively grab Sr(II) from concentrated nitric acid solution due to the size match, but they suffer from the high leakage into the liquid phase caused by the presence of a large number of hydrophilic groups. To reduce their leakage, two novel porous silica-based adsorbents, (DtBuCH18C6 + Dodec)/SiAaC-g-ABSA and (DtBuCH18C6 + Dodec)/SiAaC-g-3-ABSA, were prepared by vacuum impregnation with organic contents of about 55.9 wt.% and 56.1 wt.%, respectively. The two adsorbents have good reusability and structural stability, and the total organic carbon leakage rates in 2 M HNO_3 solution are lower than 0.56 wt.% and 0.29 wt.%, respectively. Batch adsorption experiments revealed that the two adsorbents possessed good adsorption selectivity towards Sr, with $SF_{Sr/M}$ over 40, except that of $SF_{Sr/Ba}$ in 2 M HNO_3 solution. The adsorption equilibrium of Sr in 2 M HNO_3 solution was reached within 1 h, with saturated adsorption capacities of 36.9 mg/g and 37.5 mg/g, respectively. Furthermore, the XPS results indicate that the adsorption mechanism is the coordination of the crown ether ring with Sr. This work not only develops two novel adsorbents for the separation of Sr in nitric acid environments; it also provides a method for effectively reducing the water solubility of crown ethers.

Keywords: strontium; adsorption; crown ethers; high-level liquid waste

Citation: Liu, C.; Zhang, S.; Wang, X.; Chen, L.; Yin, X.; Hamza, M.F.; Wei, Y.; Ning, S. Preparation of Two Novel Stable Silica-Based Adsorbents for Selective Separation of Sr from Concentrated Nitric Acid Solution. *Metals* **2024**, *14*, 627. https://doi.org/10.3390/met14060627

Academic Editor: Antonije Onjia

Received: 26 April 2024
Revised: 19 May 2024
Accepted: 21 May 2024
Published: 25 May 2024

1. Introduction

Nuclear energy plays an increasingly important role in the restructuring of energy sources because of its cleanliness and high efficiency [1]. The development of nuclear energy will inevitably produce large quantities of nuclear spent fuel. The PUREX process (plutonium uranium recovery by extraction) effectively separates U and Pu from nuclear spent fuel, while other fission products, including minor actinides (Np, Am, and Cm), long-lived fission products (^{99}Tc, ^{129}I, etc.), and high heat-generating elements (^{90}Sr and ^{137}Cs), are retained in the high-level liquid waste (HLLW) [2,3]. The minor actinides and long-lived fission products can be converted into short-lived or stabilized nuclides through partitioning and transmutation strategies, which can effectively shorten the potential threat time of HLLW [4]. However, the radiological and biochemical toxicity of

other nuclides, such as ^{90}Sr, still exists in the HLLW, which will have a significant negative impact on the vitrification of HLLW. Therefore, it is necessary to remove ^{90}Sr from HLLW prior to the vitrification process.

HLLWs are characterized by high radioactivity, multiple components, and high acidity, which makes the efficient separation of ^{90}Sr ($T_{1/2}$ = 28.8 a) from it extremely challenging [5–7]. Crown ethers and their derivatives carry cavities that can coordinate with Sr in high-concentration nitric acid environments and have the potential to separate Sr from HLLW [8–10]. However, the extraction of Sr by crown ethers and their derivatives usually requires the consumption of large quantities of organic diluents, which will inevitably generate a large amount of organic waste. In contrast, organic–inorganic hybrid adsorbent materials prepared by impregnating organic ligands into stabilized carriers combine the excellent properties of organic ligands with the stability of carriers and produce almost no organic waste [11–13]. Chen et al. [14] prepared a novel silica-based adsorbent by impregnating 4′,4″(5″)-di-tert-butyldicyclohexano-18-crown-6 (DtBuCH18C6) into the interior of the porous carrier (SiO_2-P), which had an adsorption capacity of 0.43 mmol/g of Sr in 2 M HNO_3 solution. However, the presence of a large number of oxygen atoms in the structure of the crown ether leads to its high hydrophilicity, which makes it prone to leakage when adsorbing Sr (II) [14].

To address the above issues, researchers have modified crown ethers to reduce their leakage in the aqueous phase. Several organic ligands, such as 1-dodecanol, tri-n-butyl phosphate, and dodecyl benzenesulfonic acid, are prone to form hydrogen bonds with crown ethers, and impregnating them into porous carriers can effectively reduce the leakage of crown ethers and thus improve the adsorption efficiency of Sr [15–17]. The modification of crown ethers' adsorbents using silica-based hybrid carriers could be applied to separate Sr in nitric acid environments.

But as with the existence of hydrophilic sulfonic acid group, the total organic carbon (TOC) in the liquid phase was still high due to the leakage of organic content from the adsorbent during the adsorption process, which needs to be further improved [17]. In this work, we investigated the static and dynamic adsorption properties of two novel stable silica-based adsorbents, (DtBuCH18C6 + Dodec)/SiAaC-g-ABSA and (DtBuCH18C6 + Dodec)/SiAaC-g-3-ABSA, by batch and column experiments on the two adsorbents on Sr. This material is different from the material in previous studies that was only impregnated with DtBuCH18C6 and dodecanol to the carrier SiO_2-P [14]. In this work, aminobenzene sulfonic acid (ABSA) and 3-aminobenzene sulfonic acid (3-ABSA) were grafted onto the previously synthesized SiAaC and then impregnated with DtBuCH18C6 and dodecanol to further improve the stability and adsorption properties of the materials [18]. The experimental data were fitted and analyzed to obtain the main adsorption parameters. The reusability and structural stability of the two adsorbents were studied. Finally, the XPS technique was used to study the change in binding energy of functional groups before and after adsorption to reveal the adsorption mechanism.

2. Experimental

2.1. Chemicals

4′,4″(5″)-di-tert-butyldicyclohexano-18-crown-6 (DtBuCH18C6, 90%) was purchased from Sigma-Aldrich (Shanghai, China). Dimethyl sulfoxide (DMSO, AR), 3-(diethoxyphosphoryloxy)-1,2,3-benzotriazin-4(3H)-one (DEPBT, 98%), 1-dodecanol (Dodec, 98%), aminobenzene sulfonic acid (ABSA, AR), and 3-aminobenzene sulfonic acid (3-ABSA, 98%) were purchased from Shanghai Aladdin Biochemical Technology Co., Ltd., (Aladdin Industrial, Inc., Shanghai, China). Other chemicals, including $Sr(NO_3)_2{\cdot}6H_2O$, used in this work were analytical grade and purchased from Shanghai Macklin Biochemical Technology Co., Ltd., (Aladdin Industrial, Inc., Shanghai, China).

2.2. Synthesis

The porous silica-based carrier SiAaC containing -COOH group was functionalized and modified to prepare two novel adsorbents, named (DtBuCH18C6 + Dodec)/SiAaC-g-ABSA and (DtBuCH18C6 + Dodec)/SiAaC-g-3-ABSA, respectively. The preparation process of SiAaC was provided in our previous work [18]. Figure 1 shows the synthesis processes of the two adsorbents. More details follow below.

SiAaC was amino-modified according to the following procedure. Firstly, 5 g of SiAaC and 50 mL of DMSO were placed in a beaker and mixed at room temperature, after which 5 g of ASAB or 3-ABSA was added. Then, 3 g catalyst of DEPBT was added to improve the grafting efficiency. The above mixed solution was stirred at 200 rpm for 12 h at room temperature. The collected products were named SiAaC-g-ABSA and SiAaC-g-3-ABSA, respectively.

(DtBuCH18C6 + Dodec)/SiAaC-g-ABSA and (DtBuCH18C6 + Dodec)/SiAaC-g-3-ABSA were prepared by the vacuum impregnation method, as detailed below. In total, 5 g of SiAaC-g-ABSA or SiAaC-g-3-ABSA was weighted and placed into a glass flask. Then, 0.9 g $DtBuCH_{18}C_6$ and 0.3 g Dodec were dissolved into 200 mL of CH_2Cl_2, and the mixture solution was added to the flask. The glass flask was fixed to a rotary evaporator (EYELA, N-300 V-WB, Tokyo, Japan) and rotated at 200 rpm. Decompression was carried out at a rate of 20 pha/10 min until the CH_2Cl_2 was completely evaporated. The collected products are named (DtBuCH18C6 + Dodec)/SiAaC-g-ABSA and (DtBuCH18C6 + Dodec)/SiAaC-g-3-ABSA, respectively.

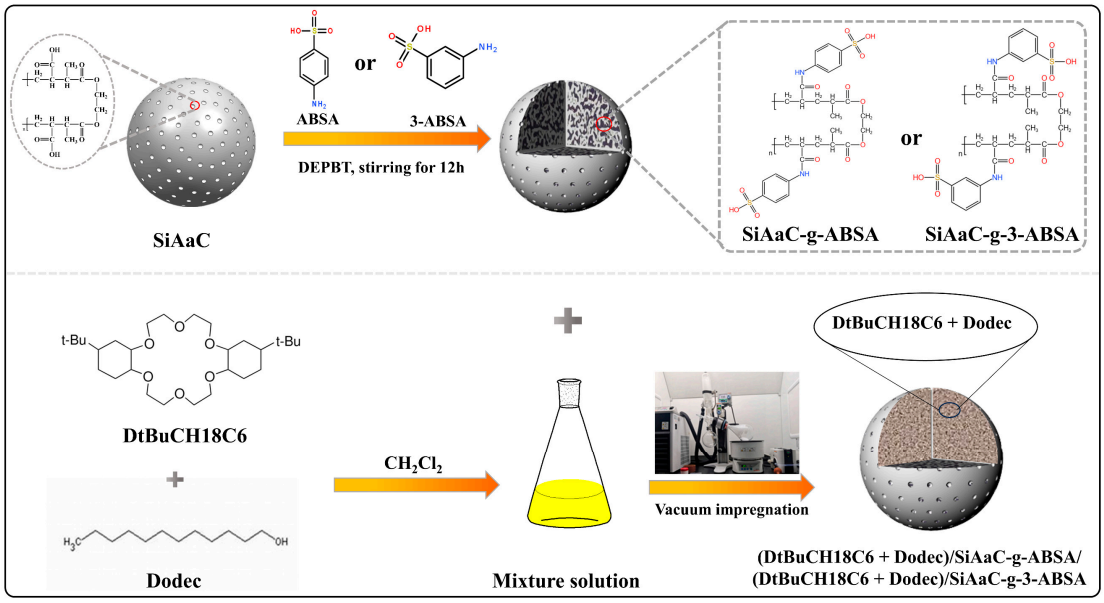

Figure 1. Schematic diagram of the preparation processes of the adsorbents.

2.3. Characterization

The SEM technique (HITACHI SU8200, Tokyo, Japan) was used to obtain the surface morphology of the adsorbents. TG-DSC analyses were conducted under an oxygen environment, using a NETZSCH STA 449F3 analyzer at a heating rate of 10 °C/min to analyze the thermal stability and component of the adsorbents (Selb, Germany). The changes in functional groups and chemical state were studied by FTIR (SHIMADZU, IRTracer-100, Tokyo, Japan) and XPS (Scalab250XI, C1s: 284.6 eV, Paris, France) analysis. The content of total organic carbon in solution was measured by a TOC analyzer (SHIMADZU, VCPH).

2.4. Batch Experiments

The adsorption performances of (DtBuCH18C6 + Dodec)/SiAaC-g-ABSA and (DtBuCH18C6 + Dodec)/SiAaC-g-3-ABSA on Sr were evaluated by batch adsorption experiments. In total, 0.1 g of the adsorbent and 5 mL HNO_3 solution containing Sr $(NO_3)_2$ were mixed in a glass vial, respectively. The vial was secured to a water-bath shaker oscillating at a rate of 160 rpm. The concentrations of Sr and other metal ions in the solution before and after adsorption were determined by atomic absorption spectrometry (AAS, SHIMADZU AA-7000, Japan) and inductively coupled plasma optical emission spectroscopy (ICP-OES, Thermo ICAP 7000, Waltham, MA, USA), respectively. The adsorption capacity Q (mg/g), adsorption efficiency E (%), distribution coefficient K_d (mL/g) and separation factor (SF) are calculated by Equations (1)– (4) [19–21]:

$$Q = \frac{(C_o - C)}{m} \times V \quad (1)$$

$$E = \frac{(C_o - C)}{C_o} \times 100\% \quad (2)$$

$$K_d = \frac{(C_o - C)}{C} \times \frac{V}{m} \quad (3)$$

$$SF_{A/B} = \frac{K_{d\,A}}{K_{d\,B}} \quad (4)$$

where C_o and C (mg/L) are the initial and equilibrium concentrations of the metal ions in the solutions, respectively; and V (mL) and m (g) are the aqueous phase volume and adsorbent mass, respectively.

2.5. Column Experiments

The dynamic adsorption behavior of (DtBuCH18C6 + Dodec)/SiAaC-g-ABSA and (DtBuCH18C6 + Dodec)/SiAaC-g-3-ABSA on Sr was investigated using column experiments, respectively. A total of 1.9981 g of the adsorbent was weighed and packed into a glass column (ϕ × h = 10 mm × 100 mm). A peristaltic pump (EYELA MP 2000, Japan) was used to pump the feed solution (C_o = 461 mg Sr/L) into the packed column at a rate of 0.5 mL/min, and the effluent was collected using a fraction collector (EYELA DC1500C, Japan). The concentration of Sr in the solution was determined by atomic absorption spectrometry (AAS, SHIMADZU AA-7000, Japan). The experimental data were fitted by the Thomas model (Equation (5)) [22,23].

$$\frac{C}{C_o} = \frac{1}{1 + exp(\frac{K_{Th}}{v}(q_o m - C_o V))} \quad (5)$$

where C_o and C are the Sr concentrations (mg/L) in the feed solution and effluent, respectively; K_{Th} (mL·g^{-1}·min^{-1}) and v (mL/min) are the Thomas constant and flow rate, respectively; q_o (mg/g) is the column adsorption capacity; and m (g) and V (mL) are the amount of adsorbent and the effluent volume.

3. Results and Discussion

3.1. Characterization of the Materials

The SEM technique was used to study the surface morphology of (DtBuCH18C6 + Dodec)/SiAaC-g-ABSA and (DtBuCH18C6 + Dodec)/SiAaC-g-3-ABSA, and the results are shown in Figure 2a,b. The two adsorbents have regular spherical morphology with a particle size of 40–100 μm. Figure 2c,d show the TG-DSC results of the two adsorbents. As the temperature increases from 25 °C to 800 °C, from the TG curves, the two adsorbents undergo mass loss until about 450 °C and then remain stable. The organic contents of

(DtBuCH18C6 + Dodec)/SiAaC-g-ABSA and (DtBuCH18C6 + Dodec)/SiAaC-g-3-ABSA are 55.9 wt.% and 56.1 wt.%, respectively. According to the DSC curves, several characteristic peaks resulting from mass decomposition are clearly observed. The characteristic peak near 100 °C originates from the evaporation of water in the adsorbents. The broad characteristic peaks between 100 °C and 496 °C derive from the thermal decomposition of organic matter in the adsorbents.

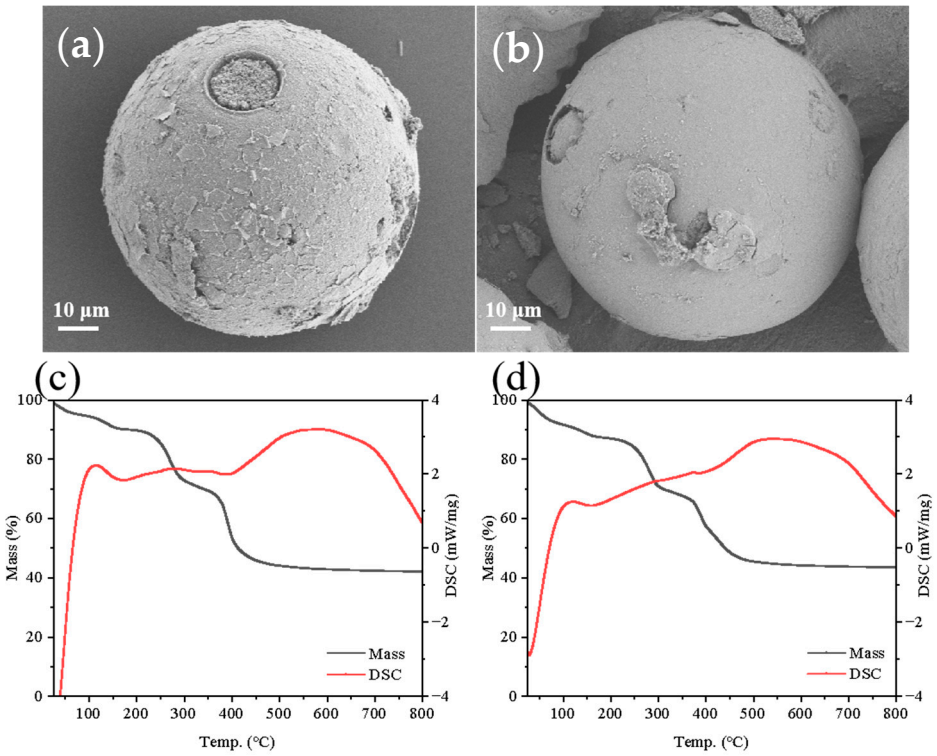

Figure 2. (**a**,**b**) SEM and (**c**,**d**) TG-DSC results of (DtBuCH18C6 + Dodec)/SiAaC-g-ABSA and (DtBuCH18C6 + Dodec)/SiAaC-g-3-ABSA.

The FTIR technique was employed to investigate the changes in functional groups during the preparation of the adsorbents, and the results are shown in Figure 3. The peaks at 469 cm^{-1}, 803 cm^{-1}, and 1096 cm^{-1} originate from the stretching vibration of the Si-O-Si [24]. After sulfonation modification of SiAaC using 3-ABSA and ABSA, the characteristic peak of S-O is observed at around 568 cm^{-1} [17]. Due to the partial overlap of the peak positions of S=O and Si-O, the S=O peak in the FTIR spectra of SiAaC-g-3-ABSA and SiAaC-g-ABSA cannot be observed as an independent peak. After the modification of SiAaC-g-3-ABSA and SiAaC-g-ABSA using DtBuCH18C6 and Dodec, the C-O-C characteristic peaks (around 1260 cm^{-1}) are significantly enhanced. The peak at 2929-2961 cm^{-1} derives from the C-H vibration [25]. The peak around 3461 cm^{-1} is from the adsorbed water [26].

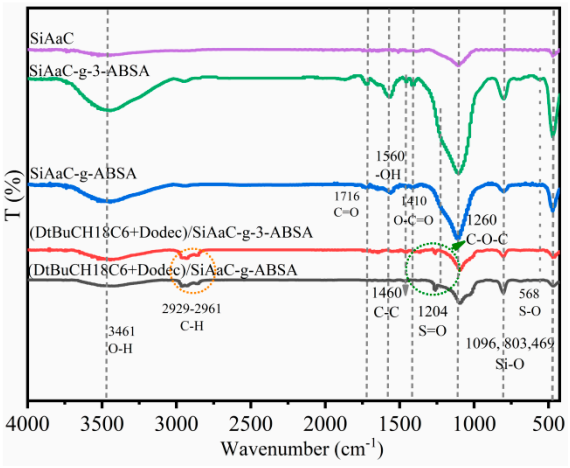

Figure 3. FTIR results of SiAaC, SiAaC-g-3-ABSA, SiAaC-g-ABSA, (DtBuCH18C6 + Dodec)/SiAaC-g-3-ABSA and (DtBuCH18C6 + Dodec)/SiAaC-g-ABSA.

3.2. Batch Adsorption Experiments

3.2.1. Adsorption Selectivity

Figure 4 shows the adsorption selectivity of Sr by (DtBuCH18C6 + Dodec)/SiAaC-g-ABSA and (DtBuCH18C6 + Dodec)/SiAaC-g-3-ABSA in simulated high-level liquid waste. At a nitric acid concentration of 0.5 M, the sulfonic acid group promotes the coordination of the crown ether ring with Sr, resulting in the two adsorbents exhibiting good adsorption of Sr [17]. As the nitric acid concentration increases to 1 M, the coordination promotion of the sulfonic acid groups to the crown ether ring is inhibited, leading to a weakening of the adsorption of Sr by the two adsorbents. As the nitric acid concentration increases to 2 M, the coordination of the crown ether ring to Sr is enhanced, leading to a rise in Sr adsorption. With the further increase in nitric acid concentration, there is competition adsorption of nitric acid with Sr, resulting in the weakening of the adsorption of Sr by the two adsorbents (Equations (6)–(8)). In addition, the two adsorbents show weak adsorption on Ba and Pd in the simulated high-level liquid waste in Figure 4, and almost no adsorption for other metal ions, with $SF_{Sr/M}$ over 40, except that of $SF_{Sr/Ba}$ in the simulated high-level liquid waste of 2 M HNO_3. It indicates good adsorption selectivity of the two adsorbents on Sr.

$$Sr^{2+} + 2RSO_3^- + DtBuCH18C6 \leftrightarrow Sr(RSO_3)_2 \cdot DtBuCH18C6 \quad (6)$$

$$Sr^{2+} + 2NO_3^- + DtBuCH18C6 \leftrightarrow Sr(NO_3)_2 \cdot DtBuCH18C6 \quad (7)$$

$$HNO_3 + DtBuCH18C6 \leftrightarrow HNO_3 \cdot DtBuCH18C6 \quad (8)$$

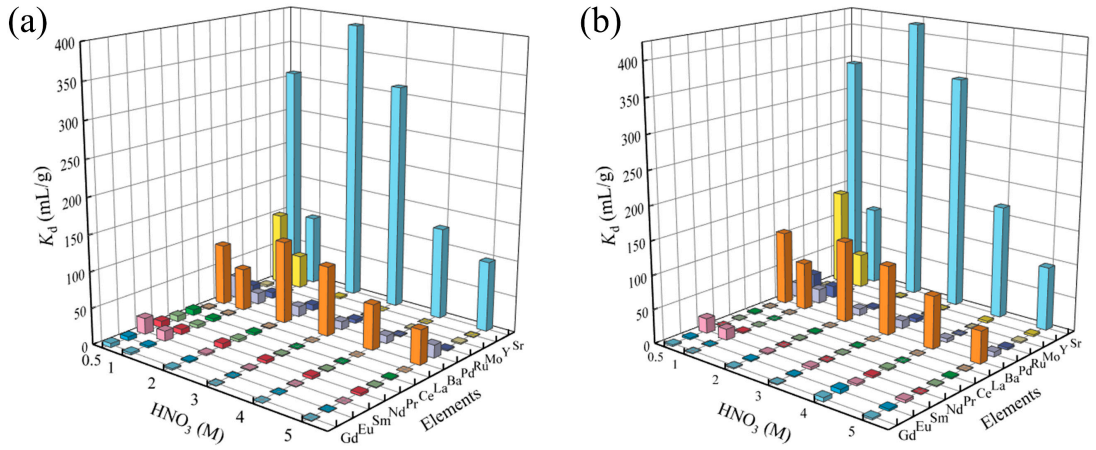

Figure 4. Adsorption selectivity of (**a**) (DtBuCH18C6 + Dodec)/SiAaC-g-ABSA and (**b**) (DtBuCH18C6 + Dodec)/SiAaC-g-3-ABSA on Sr in different HNO_3 concentrations ([M] = 1 mM, m/V = 0.1 g/ 5 mL, t = 6 h, T = 298 K).

3.2.2. Kinetics

The adsorption kinetics of (DtBuCH18C6 + Dodec)/SiAaC-g-ABSA and (DtBuCH18C6 + Dodec)/SiAaC-g-3-ABSA on Sr in 2 M HNO_3 solution were studied. According to Figure 5, with the increase in adsorption time, the adsorption of Sr by the adsorbent first increased rapidly and then remained stable. The adsorption equilibriums of Sr by the two adsorbents obtained within 1 h with the adsorption capacities were about 36.9 mg/g and 37.5 mg/g.

Moreover, a pseudo-second-order kinetics model (Equation (9)) was adopted to analyze the experimental data [27]. The results are shown in Figure 5 and Table 1. The correlation coefficients (R^2) were higher than 0.99, indicating the good applicability of the pseudo-second-order model to the adsorption processes. Therefore, it can be hypothesized that the adsorption of Sr by the two adsorbents is chemisorption [28,29].

$$Q_t = \frac{k_2 Q_e^2 t}{1 + k_2 Q_e t} \quad (9)$$

where Q_e and Q_t (mg/g) are equilibrium and adsorption capacities at time, t (min), respectively; k_2 (min^{-1}) is the adsorption rate constants of pseudo-second order.

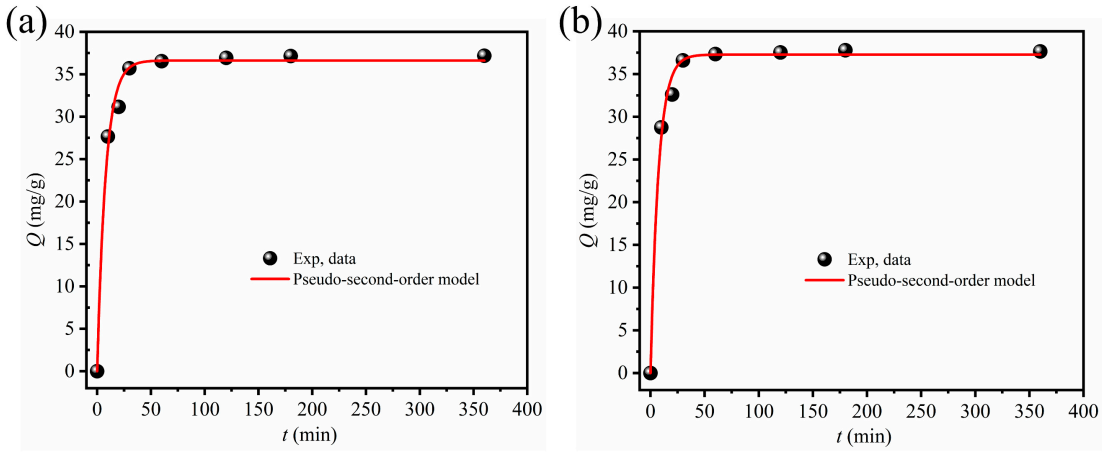

Figure 5. Adsorption kinetics of (**a**) (DtBuCH18C6 + Dodec)/SiAaC-g-ABSA and (**b**) (DtBuCH18C6 + Dodec)/SiAaC-g-3-ABSA on Sr in 2 M HNO_3 concentration (C_o = 5 mM, m/V = 0.1 g/5 mL, T = 298 K).

Table 1. Kinetics parameters of Sr by the two adsorbents.

T (K)	Adsorbents	Pseudo-Second-Order Model		
		K_2 (g·h/mg)	Q_e (mg/g)	R^2
298	(DtBuCH18C6 + Dodec)/SiAaC-g-ABSA	0.13	36.6	0.99
	(DtBuCH18C6 + Dodec)/SiAaC-g-3-ABSA	0.14	37.4	0.99

3.2.3. Isotherms

The adsorption isotherms of Sr by (DtBuCH18C6 + Dodec)/SiAaC-g-ABSA and (DtBuCH18C6 + Dodec)/SiAaC-g-3-ABSA in 2 M HNO_3 solution were studied by varying the initial Sr concentration of the solution, with the results shown in Figure 6. The adsorption of Sr by the two adsorbents increased significantly with the increase in the equilibrium ion concentration, and the maximum adsorption capacity was about 39.1 mg/g and 39.2 mg/g, respectively.

Moreover, Langmuir and Freundlich isotherm models were applied to analyze the experimental data [30–32]. The results are shown in Figure 6 and Table 2. According to the fitting results, the Langmuir model has a higher correlation coefficient (R^2 = 0.99) compared to the Freundlich model, indicating that the Langmuir model has better applicability to the adsorption process. Therefore, it can be concluded that the adsorption of Sr by the two adsorbents is monomolecular layer chemisorption [24,33,34].

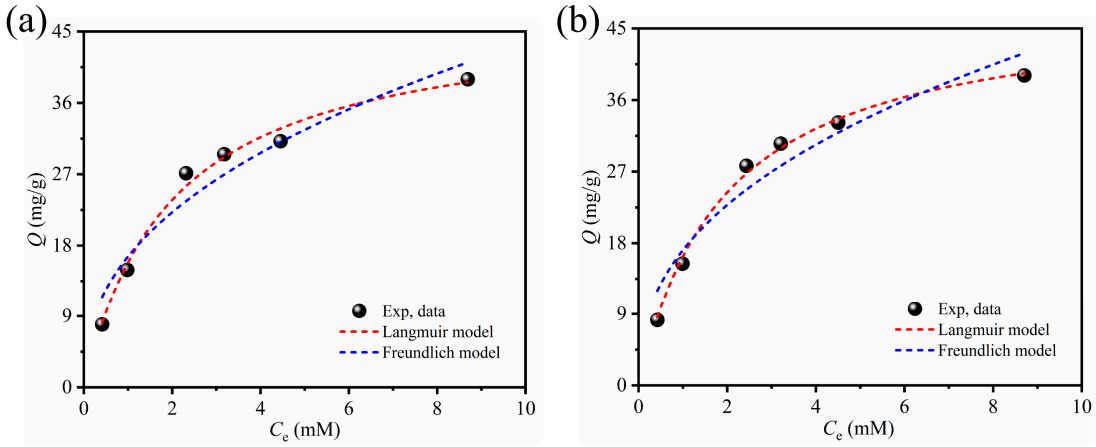

Figure 6. Adsorption isotherms of (**a**) (DtBuCH18C6 + Dodec)/SiAaC-g-ABSA and (**b**) (DtBuCH18C6 + Dodec)/SiAaC-g-3-ABSA on Sr in 2 M HNO_3 concentration (m/V = 0.1 g/5 mL, T = 298 K).

$$Q_e = \frac{q_m \times K_L \times C_e}{1 + K_L \times C_e} \tag{10}$$

$$Q_e = K_F \times C_e^{\frac{1}{n}} \tag{11}$$

where q_m (mg/g) is the calculated saturation adsorption capacity; C_e (mM) is the equilibrium ions concentration; K_L (L/mg) and K_F ($mg^{1-n} \cdot L^n/g$) are the Langmuir and Freundlich model constants, respectively; and n is the adsorption intensity.

Table 2. Isotherms parameters of Sr by the two adsorbents.

Adsorbents	Langmuir Model			Freundlich Model		
	K_L (L/mg)	q_m (mg/g)	R^2	n	K_F (mg^{1-n}·L^n/g)	R^2
(DtBuCH18C6 + Dodec)/SiAaC-3-ABSA	0.50	47.4	0.99	0.50	16.6	0.94
(DtBuCH18C6 + Dodec)/SiAaC-g-3-ABSA	0.51	48.2	0.99	0.4	17.1	0.93

3.3. Reusability and Stability

To effectively assess the utility of (DtBuCH18C6 + Dodec)/SiAaC-g-ABSA and (DtBuCH18C6 + Dodec)/SiAaC-g-3-ABSA, the reusability of the two adsorbents was studied. The desorption capacity, Q_d (mg/g), and desorption efficiency, E_d (%), are calculated by Equation (12) and Equation (13), respectively[28]:

$$Q_d = C_d \times \frac{V}{m} \quad (12)$$

$$E_d = Q_d/Q \times 100\% \quad (13)$$

where C_d (mg/L) means the concentration of Sr in the desorption solution.

According to Figure 7, pure water is able to effectively desorb the adsorbed Sr by the two adsorbents with the desorption efficiencies of about 77% and 82%, respectively. The adsorption efficiency of the adsorbent for Sr decreases a little as the number of adsorption–desorption cycles increases. After five adsorption–desorption cycles, the adsorption efficiencies of the adsorbent for Sr are still kept at about 57% and 75%, and the desorption efficiencies are 78% and 85%, respectively. The above results indicate that the two adsorbents have good reusability.

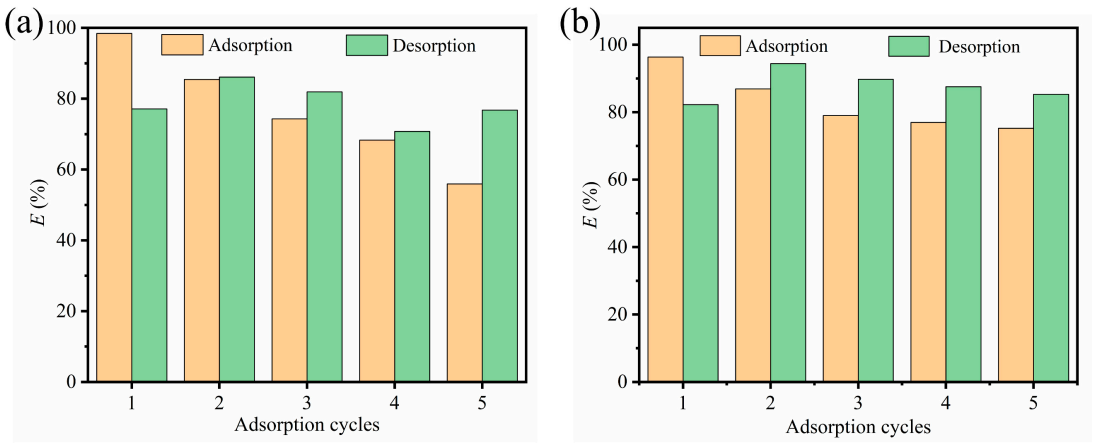

Figure 7. Reusability of (**a**) (DtBuCH18C6 + Dodec)/SiAaC-g-ABSA and (**b**) (DtBuCH18C6 + Dodec)/SiAaC-g-3-ABSA on Sr in 2 M HNO_3 concentration (C_o = 5 mM, m/V = 0.1 g/5 mL, t = 180 min, T = 298 K).

The structural stability of the two adsorbents was investigated by determining the total organic carbon (TOC) content in the aqueous phase. The TOC leakage of the two adsorbents in different concentrations of nitric acid solutions is shown in Figure 8. In 0.1–5 M nitric acid solutions, the TOC leakages of the two adsorbents are less than 188 ppm and 95 ppm, respectively. The calculated TOC leakage rates for (DtBuCH18C6 + Dodec)/SiAaC-g-ABSA and (DtBuCH18C6 + Dodec)/SiAaC-g-3-ABSA are less than 0.56 wt.% and 0.29 wt.%, respectively, indicating the good structural stability of the two adsorbents. In this study, the leakage rate of organic compounds is significantly reduced compared to that in previous work [17].

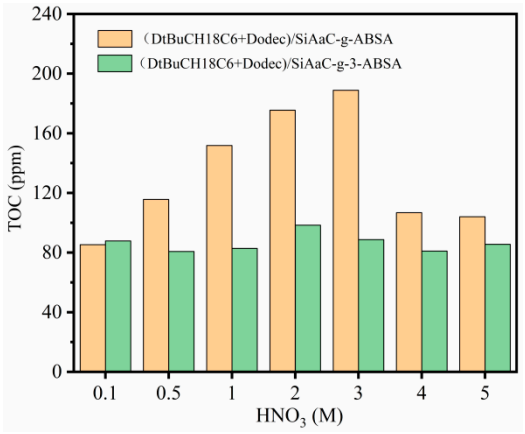

Figure 8. TOC leakage of the two adsorbents in different concentrations of HNO_3 solutions. (Contact time: 24 h, m/V = 0.1 g/5 mL, and T = 298 K).

Figure 9 explains to us that this reduction in leakage rate is attributed to the intermolecular bonding between the -SO3H group introduced through grafting and DtBuCH18C6 through hydrogen bonding in our study. Modifiers that can form hydrogen bonds with DtBuCH18C6 can effectively reduce the leakage of the latter in the solution, which has been confirmed in previous studies [16]. Furthermore, (DtBuCH18C6 + Dodec)/SiAaC-g-3-ABSA exhibits a lower leakage rate compared to (DtBuCH18C6 + Dodec)/SiAaC-g-ABSA. This is attributed to the higher grafting efficiency of 3-ABSA in the former, which enhances the protection of the modifier on DtBuCH18C6 and further improves the reusability of the material.

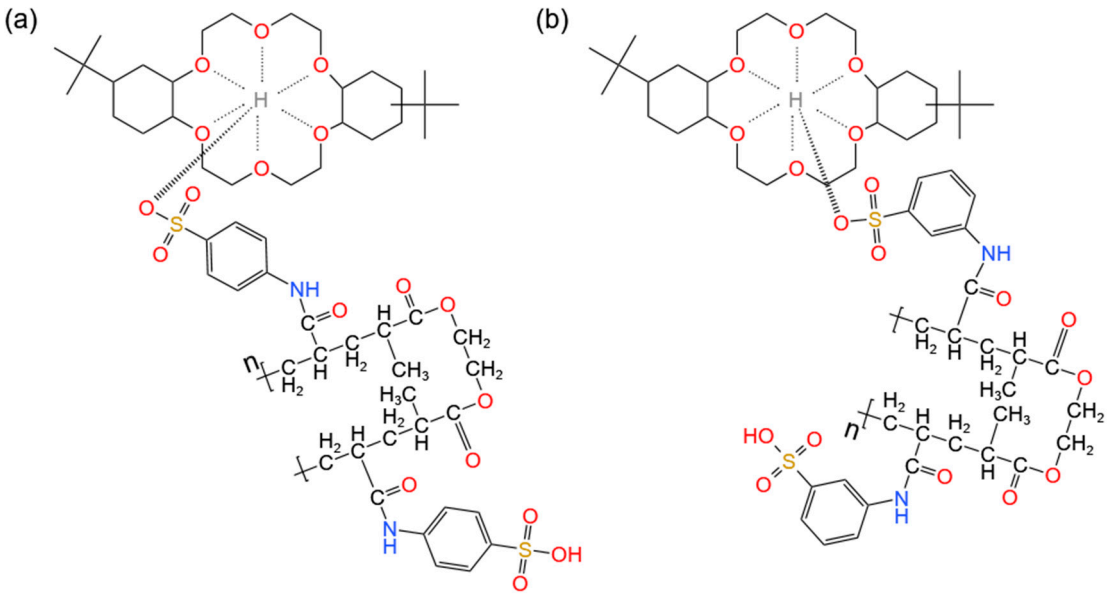

Figure 9. The intermolecular binding of DtBuCH18C6 to (**a**) (DtBuCH18C6 + Dodec)/SiAaC-g-ABSA and (**b**) (DtBuCH18C6 + Dodec)/SiAaC-g-3-ABSA via hydrogen bonds, respectively.

3.4. Column Experiments

The dynamic adsorption behavior of Sr by two adsorbents was investigated, and the breakthrough curves were fitted using the Thomas model [35]. According to Figure 9, the Sr in the effluent is observed when the effluent volume exceeds 70 mL and 85 mL, respectively. After that, the breakthrough curves climb rapidly, and the two adsorbents reach saturation adsorption when the effluent volumes are higher than 139 mL and 154 mL, respectively. Based on the fitting results of the Thomas model in Figure 10, the correlation

coefficients, R^2, are close to 1, indicating that the model has good applicability to the dynamic adsorption process. The dynamic adsorption capacities of the two adsorbents for Sr are about 30.2 mg/g and 35.5 mg/g, respectively, while the theoretical adsorption capacities fitted by the Thomas model are 41.6 mg/g and 42.4 mg/g, respectively. The discrepancy between the theoretical Q and actual Q is likely caused by the fluctuation of the flow rate during the adsorption process [36].

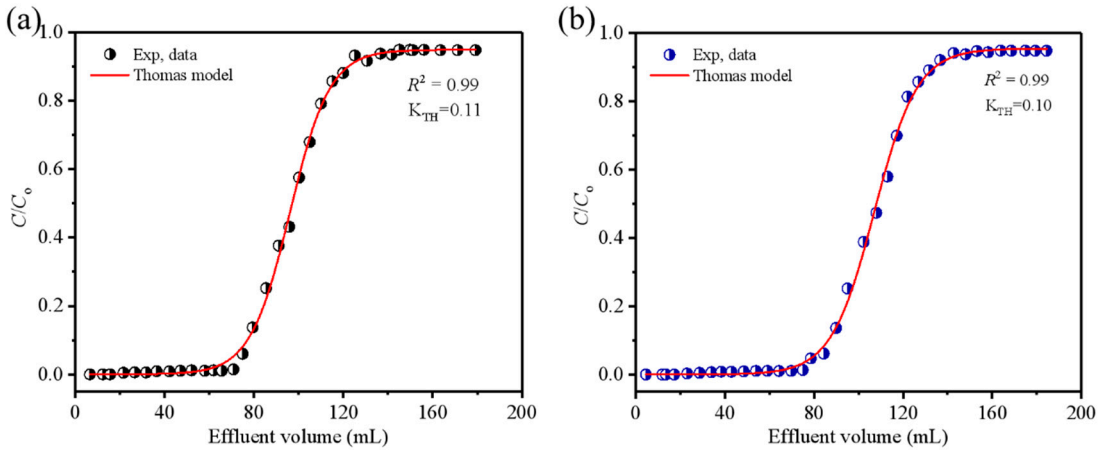

Figure 10. Breakthrough curves of (**a**) (DtBuCH18C6 + Dodec)/SiAaC-3-ABSA and (**b**) (DtBuCH18C6 + Dodec)/SiAaC-g-3-ABSA on Sr in 2 M HNO_3 concentration (C_o = 461 mg/L, m = 1.9981 g, ϕ × h = 10 mm × 100 mm, flow speed = 0.5 mL/min, T = 298 K).

3.5. Mechanism Study

XPS analysis was used to study the adsorption mechanism. Figure 11 shows the XPS results of the (DtBuCH18C6 + Dodec)/SiAaC-g-ABSA and (DtBuCH18C6 + Dodec)/SiAaC-g-3-ABSA before and after adsorption of Sr from 2 M HNO_3 solution. After the adsorption of Sr by the two adsorbents, the characteristic peak of Sr 3d was detected in the full XPS spectra (Figure 11a,d). According to the fitting results in Figure 11b,e, Sr 3d can be divided into Sr 3d 3/2 and Sr 3d 5/2, with the binding energies of about 135.6 eV and 133. 8 eV, respectively [37–39]. According to previous reports [40,41], crown ethers are susceptible to coordination interactions, with Sr leading to more pronounced changes in C 1s binding energy. Therefore, in the present work, the changes in C 1s binding energy before and after the adsorption of Sr by the two adsorbents were investigated. According to the XPS results in Figure 11c,f, C 1s can be divided into three forms, i.e., C-C, C-O-C, and C=O, with the binding energies of 284.79 eV, 285.17 eV, and 286.22 eV for (DtBuCH18C6 + Dodec)/SiAaC-g-ABSA and 284.81 eV, 285.41 eV, and 286.41 eV for (DtBuCH18C6 + Dodec)/SiAaC-g-3-ABSA, respectively [18,27]. After the adsorption of Sr by the two adsorbents, the binding energy of C-O-C shifted to 284.88 eV and 285.41 eV, respectively. The change in C-O-C binding energy after adsorption is presumed to be caused by the coordination between the crown ether ring and Sr [27].

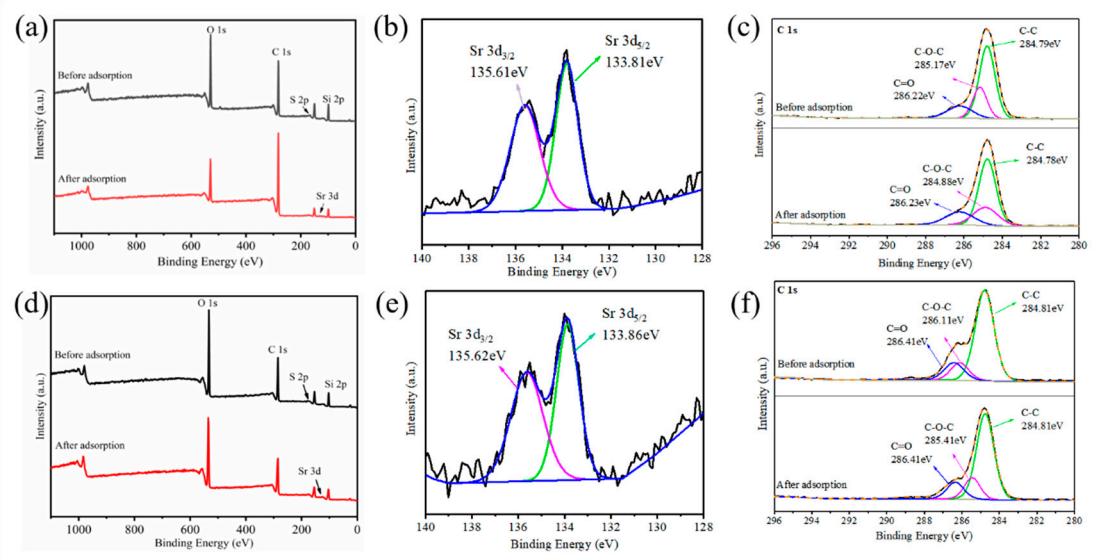

Figure 11. XPS results of (**a**–**c**) (DtBuCH18C6 + Dodec)/SiAaC-3-ABSA and (**d**–**f**) (DtBuCH18C6 + Dodec)/SiAaC-g-3-ABSA before and after adsorption of Sr.

3.6. Comparison of (DtBuCH18C6 + Dodec)/SiAaC-g-ABSA and (DtBuCH18C6 + Dodec)/SiAaC-g-3-ABSA with Other Materials

In practical applications, utility and cost-effectiveness are paramount. A comparison of various solid adsorbent materials is presented in Table 3. The prepared (DtBuCH18C6 + Dodec)/SiAaC-g-ABSA and (DtBuCH18C6 + Dodec)/SiAaC-g-3-ABSA exhibit high K_d values, complete desorption, excellent reusability, and high selectivity. In summary, both (DtBuCH18C6 + Dodec)/SiAaC-g-ABSA and (DtBuCH18C6 + Dodec)/SiAaC-g-3-ABSA are well-suited for the treatment of Sr.

Table 3. Comparison of (DtBuCH18C6 + Dodec)/SiAaC-3-ABSA and (DtBuCH18C6 + Dodec)/SiAaC-g-3-ABSA with other materials.

Adsorbents	Other Species	C(HNO_3)	K_d (cm^3/g)	Reusability	Ref.
(DtBuCH18C6 + [C2mim] [NTf2])/SiO_2-P	Sr, Ba, Na, Ca, La, Nd, Sm, Gd, Ru, Pd, Zr, Mo	3 M	30	–	[42]
(DtBuCH18C6 + Oct)/SiO_2- P	Ru, Pd, Ba, Mo, La, Y, Cs, Na, K	2 M	<200	–	[43]
(DtBuCH18C6 + Dodec)/SiO_2-P	Cs, Ru, Pd, La, Nd, Sm, Gd, Zr, Mo	3 M	182.0	–	[11]
(DtBuCH18C6 + Dodec +DBS)/ SiO_2-P	–	3 M	260.3	–	[17]
(DtBuCH18C6 + Dodec)/SiAaC-g-ABSA	Gd, Eu, Sm, Nd, Pr, Ce, La, Ba, Pd, Ru, Mo, Y	2 M	389.68	4	This study
(DtBuCH18C6 + Dodec)/SiAaC-g-3-ABSA		2 M	416.68	≥5	

4. Conclusions

In this work, two novel silica-based adsorbents (DtBuCH18C6 + Dodec)/SiAaC-g-ABSA and (DtBuCH18C6 + Dodec)/SiAaC-g-3-ABSA were prepared successively by chemical grafting and vacuum impregnation for the selective separation of Sr in nitric acid environment. Different from the previous research work (DtBuCH18C6 + dodecanol)/SiO_2-P materials, SiAaC-g-ABSA and SiAaC-g-3-ABSA were used as carriers in

this work, respectively. And the new supports can further improve the stability and adsorption properties of the materials. The formation of hydrogen bonds between the -SO3H groups introduced through grafting in our study and DtBuCH18C6 further reduces the leakage of the latter in the solution. The two adsorbents exhibited good adsorption selectivity for Sr in 0.5–5 M HNO_3 solutions with the separation factor, $SF_{Sr/M}$, over 40, except that of $SF_{Sr/Ba}$. The adsorption of Sr matched well with pseudo-second-order and Langmuir model with the saturated adsorption capacities of 36.9 mg/g and 37.5 mg/g obtained within 1 h, respectively. The adsorbed Sr could be desorbed efficiently using pure water with desorption efficiencies of 77% and 82%, respectively. They possess good reusability with Sr adsorption efficiencies of about 57% and 75%, respectively, after five adsorption–desorption cycles. The leakage rates for the two adsorbents in the liquid phase were less than 0.56 wt.% and 0.29 wt.%, respectively, according to the TOC analysis, indicating the good structural stability of the two adsorbents. In column experiments, the dynamic adsorption capacities of the two adsorbents for Sr were about 30.2 mg/g and 35.5 mg/g, respectively. Finally, the XPS results indicate that the adsorption mechanism is the coordination between the adsorbents and Sr.

Author Contributions: Conceptualization, C.L., X.Y., L.C. and M.F.H.; Methodology, C.L. and X.W.; Validation, Y.W.; Formal analysis, C.L. and S.Z.; Investigation, C.L., L.C., X.W.; Resources, X.W.; Data curation, C.L.; Writing—original draft preparation, C.L.; Writing—review and editing, S.Z., X.W., L.C., M.F.H., Y.W. and S.N.; Visualization, C.L.; Supervision, L.C., X.Y., M.F.H., Y.W. and S.N.; Project administration, S.N.; Funding acquisition, S.N. All authors have read and agreed to the published version of the manuscript.

Funding: This work was supported by the National Natural Science Foundation of China (12275124) and the Science and Technology Innovation Program of Hunan Province (2023RC1067).

Data Availability Statement: The data presented in this study are available on request from the corresponding author. As the project is still ongoing, the data will not be disclosed due to the needs of the project.

Conflicts of Interest: The authors declare that they have no known competing financial interests or personal relationships that could have appeared to influence the work reported in this paper.

References

1. Xu, Y.; Kim, S.Y.; Ito, T.; Nakazawa, K.; Funaki, Y.; Tada, T.; Hitomi, K.; Ishii, K. Adsorption and separation behavior of yttrium and strontium in nitric acid solution by extraction chromatography using a macroporous silica-based adsorbent. *J. Chromatogr. A* **2012**, *1263*, 28–33. https://doi.org/10.1016/j.chroma.2012.09.036.
2. Venkatesan, K.A.; Selvan, B.R.; Antony, M.P.; Srinivasan, T.G.; Rao, P.R.V. Extraction of palladium from nitric acid medium by commercial resins with phosphinic acid, methylene thiol and isothiouronium moieties attached to polystyrene-divinylbenzene. *J. Radioanal. Nucl. Ch.* **2005**, *266*, 431–440. https://doi.org/10.1007/s10967-005-0928-x.
3. Khan, P.N.; Bhattacharyya, A.; Banerjee, D.; Sugilal, G.; Kaushik, C.P. Partitioning of heat generating fission product (^{137}Cs & ^{90}Sr) from acidic medium by 1,3-dioctyloxy-calix[4]arenecrown-6 (CC6) & Octabenzyloxyoctakis[[[(N,N-diethylamino)carbonyl)]methyl]oxy]calix[8]arene (BOC8A) in nitro octane diluent: Batch scale study & process parameter optimization. *Sep. Purif. Technol*. **2021**, *274*, 119102. https://doi.org/10.1016/j.seppur.2021.119102.
4. Xiao, C.L.; Wang, C.Z.; Yuan, L.Y.; Li, B.; He, H.; Wang, S.; Zhao, Y.L.; Chai, Z.F.; Shi, W.Q. Excellent selectivity for actinides with a tetradentate 2,9-diamide-1,10-phenanthroline ligand in highly acidic solution: A hard–soft donor combined strategy. *Inorg. Chem.* **2014**, *53*, 1712–1720. https://doi.org/10.1021/ic402784c.
5. Xu, L.; Zhang, A.; Pu, N.; Xu, C.; Chen, J. Development of Two novel silica based symmetric triazine-ring opening N-donor ligands functional adsorbents for highly efficient separation of palladium from HNO_3 solution. *J. Hazard. Mater.* **2019**, *376*, 188–199. https://doi.org/10.1016/j.jhazmat.2019.05.028.
6. Datta, S.J.; Oleynikov, P.; Moon, W.K.; Ma, Y.; Mayoral, A.; Kim, H.; Dejoie, C.; Song, M.K.; Terasaki, O.; Yoon, K.B. Removal of ^{90}Sr from highly Na^+-rich liquid nuclear waste with a layered vanadosilicate. *Energ. Environ. Sci.* **2019**, *12*, 1857–1865. https://doi.org/10.1039/c8ee03302a.
7. Zhang, M.; Gu, P.; Yan, S.; Pan, S.; Dong, L.; Zhang, G. A novel nanomaterial and its new application for efficient radioactive strontium removal from tap water: KZTS-NS metal sulfide adsorbent versus CTA-F-MF process. *Chem. Eng. J.* **2020**, *391*, 123486. https://doi.org/10.1016/j.cej.2019.123486.

8. Song, Y.; Du, Y.; Lv, D.; Ye, G.; Wang, J. Macrocyclic receptors immobilized to monodisperse porous polymer particles by chemical grafting and physical impregnation for strontium capture: A comparative study. *J. Hazard. Mater.* **2014**, *274*, 221–228. https://doi.org/10.1016/j.jhazmat.2014.04.010.
9. Saha, D.; Vithya, J.; Kumar, R.; Joseph, M. Studies on purification of ^{89}Sr from irradiated yttria target by multi-column extraction chromatography using DtBuCH18-C-6/XAD-7 resin. *Radiochim. Acta* **2019**, *107*, 479–487. https://doi.org/10.1515/ract-2018-2997.
10. Yi, R.; Xu, C.; Sun, T.; Wang, Y.; Ye, G.; Wang, S.; Chen, J. Improvement of the extraction ability of bis(2-propyloxy)calix[4]arene-crown-6 toward cesium cation by introducing an intramolecular triple cooperative effect. *Sep. Purif. Technol.* **2018**, *199*, 97–104. https://doi.org/10.1016/j.seppur.2018.01.051.
11. Wu, Y.; Kim, S.-Y.; Tozawa, D.; Ito, T.; Tada, T.; Hitomi, K.; Kuraoka, E.; Yamazaki, H.; Ishii, K. Equilibrium and kinetic studies of selective adsorption and separation for strontium using DtBuCH18C6 loaded resin. *J. Nucl. Sci. Technol.* **2012**, *49*, 320–327. https://doi.org/10.1080/00223131.2012.660022.
12. Zhang, A.; Xiao, C.; Chai, Z. SPEC Process II. Adsorption of strontium and some typical co-existent elements contained in high level liquid waste onto a macroporous silica-based crown ether impregnated functional composite. *J. Radioanal. Nucl. Chem.* **2009**, *280*, 181–191. https://doi.org/10.1007/s10967-008-7411-4.
13. Guo, C.; Yuan, M.; He, L.; Cheng, L.; Wang, X.; Shen, N.; Ma, F.; Huang, G.; Wang, S. Efficient capture of Sr2+from acidic aqueous solution by an 18-crown-6-etherbased metal organic framework. *CrystEngComm* **2021**, *23*, 3349–3355. https://doi.org/10.1039/D1CE00229E.
14. Chen, Z.; Wu, Y.; Wei, Y. Adsorption characteristics and radiation stability of a silica-based DtBuCH18C6 adsorbent for Sr (II) separation in HNO_3 medium. *J. Radioanal. Nucl. Ch.* **2014**, *299*, 485–491. https://doi.org/10.1007/s10967-013-2750-1.
15. Sharma, J.N.; Khan, P.N.; Dhami, P.S.; Jagasia, P.; Tessy, V.; Kaushik, C.P. Separation of strontium-90 from a highly saline high level liquid waste solution using 4,4′(5′)-[di-tert-butyldicyclohexano]-18-crown-6 + isodecyl alcohol/n-dodecane solvent. *Sep. Purif. Technol.* **2019**, *229*, 115502. https://doi.org/10.1016/j.seppur.2019.04.032.
16. Zhang, A.; Xiao, C.; Kuraoka, E.; Kumagai, M. Preparation of a novel silica-based DtBuCH18C6 impregnated polymeric composite modified by tri-n-butyl phosphate and its application in chromatographic partitioning of strontium from high level liquid waste. *Ind. Eng. Chem. Res.* **2007**, *46*, 2164–2171. https://doi.org/10.1021/ie061404o.
17. Wang, Y.; Wen, Y.; Mao, C.; Sang, H.; Wu, Y.; Li, H.; Wei, Y. Development of chromatographic process for the dynamic separation of ^{90}Sr from high level liquid waste through breakthrough curve simulation and thermal analysis. *Sep. Purif. Technol.* **2022**, *282*, 120103. https://doi.org/10.1016/j.seppur.2021.120103.
18. Liu, H.; Ning, S.; Zhang, S.; Wang, X.; Chen, L.; Fujita, T.; Wei, Y. Preparation of a mesoporous ion-exchange resin for efficient separation of palladium from simulated electroplating wastewater. *J. Environ. Chem. Eng.* **2022**, *10*, 106966. https://doi.org/10.1016/j.jece.2021.106966.
19. Ma, F.Y.; Li, Z.; Zhou, W.; Li, Q.N.; Zhang, L. Application of polyantimonic acid-polyacrylonitrile for removal of strontium (II) from simulated high-level liquid waste. *J. Radioanal. Nucl. Chem.* **2017**, *311*, 2007–2013. https://doi.org/10.1007/s10967-016-5150-5.
20. Ning, S.Y.; Wang, X.P.; Zou, Q.; Shi, W.Q.; Tang, F.D.; He, L.F.; Wei, Y.Z. Direct separation of minor actinides from high level liquid waste by Me_2-CA-BTP/SiO_2-P adsorbent. *Sci. Rep.* **2017**, *7*, 1–7. https://doi.org/10.1038/s41598-017-14758-2.
21. Liu, J.Q.; Liu, Y.J.; Talay, D.K.; Calverley, E.; Brayden, M.; Martinez, M. A new carbon molecular sieve for propylene/propane separations. *Carbon* **2015**, *85*, 201-211. https://doi.org/10.1016/j.carbon.2014.12.089
22. Chang, K.C.; Lo, H.-M.; Lin, K.-L.; Liu, M.-H.; Chiu, H.-Y.; Lo, F.-C.; Chang, J.H. Cu adsorption in fixed bed column with three different influent concentration. *E3S Web Conf.* **2019**, *120*, 03003. https://doi.org/10.1051/e3sconf/201912003003.
23. Unuabonah, E.I.; Omorogie, M.O.; Oladoja, N.A. Modeling in adsorption: Fundamentals and applications, Compos. *Nanoadsorbents* **2018**, 85–118. https:// doi.org/10.1016/B978-0-12-814132-8.00005-8.
24. Tian, X.; Wang, S.; Li, J.S.; Liu, F.X.; Wang, X.; Chen, H.; Ni, H.Z.; Wang, Z. Composite membranes based on polybenzimidazole and ionic liquid functional Si-O-Si network for HT-PEMFC applications. *Int. J. Hydrogen Energy* **2017**, *42*, 21913–21921. https://doi.org/10.1016/j.ijhydene.2017.07.071.
25. Kozubal, J.; Heck, T.; Metz, R.B. Vibrational Spectroscopy of Intermediates and C-H Activation Products of Sequential Zr^+ Reactions with CH_4, *J. Phys. Chem. A* **2020**, *124*, 8235–8245. https://doi.org/10.1021/acs.jpca.0c07027.
26. Dai, Y.; Liu, Y.; Zhang, A.Y. Preparation and characterization of a mesoporous polycrown impregnated silica and its adsorption for palladium from highly acid medium. *J. Porous Mater.* **2017**, *24*, 1037–1045. https://doi.org/10.1007/s10934-016-0343-4.
27. Tang, J.; Liao, L.; He, X.; Lv, L.; Yin, X.; Li, W.; Wei, Y.; Ning, S.; Chen, L. Efficient separation of radium from natural thorium using a mesoporous silica-supported composite resin with sulfonic acid groups for the acquisition of targeted α-nuclides ^{212}Pb. *Chem. Eng. J.* **2024**, *485*, 150022. https://doi.org/10.1016/j.cej.2024.150022.
28. Wang, J.; Guo, X. Adsorption kinetic models: Physical meanings, applications, and solving methods. *J. Hazard. Mater.* **2020**, *390*, 122156. https://doi.org/10.1016/j. jhazmat.2020.122156.
29. Zhang, A.Y.; Wang, W.H.; Chai, Z.F.; Kumagai, M. Separation of strontium ions from a simulated highly active liquid waste using a composite of silica-crown ether in a polymer. *J. Sep. Sci.* **2008**, *31*, 3148–3155. https://doi.org/10.1002/jssc.200800358.
30. Lu, L.; Na, C.Z. Gibbsian interpretation of Langmuir, Freundlich and Temkin isotherms for adsorption in solution. *Philos. Mag. Lett.* **2022**, *102*, 239–253. https://doi.org/10.1080/09500839.2022.2084571.

31. Ezzati, R.; Pseudo-First-Order, D.O. Derivation of Pseudo-First-Order, Pseudo-Second-Order and Modified Pseudo-First-Order rate equations from Langmuir and Freundlich isotherms for adsorption. *Chem. Eng. J.* **2020**, *392*, 123705. https://doi.org/10.1016/j.cej.2019.123705.
32. Martín, F.S.; Kracht, W.; Vargas, T. Attachment of *Acidithiobacillus ferrooxidans* to pyrite in fresh and saline water and fitting to Langmuir and Freundlich isotherms. *Biotechnol. Lett.* **2020**, *42*, 957–964. https://doi.org/10.1007/s10529-020-02842-z.
33. Ning, S.; Zhang, S.; Zhang, W.; Zhou, J.; Wang, S.; Wang, X.; Wei, Y. Separation and recovery of Rh, Ru and Pd from nitrate solution with a silica-based isoBu-BTP/SiO_2-P adsorbent. *Hydrometallurgy* **2019**, *191*, 105207. https://doi.org/10.1016/j.hydromet.2019.105207.
34. Baseri, H.; Tizro, S. Treatment of nickel ions from contaminated water by magnetit based nanocomposite adsorbents: Effects of thermodynamic and kinetic parameters and modeling with Langmuir and Freundlich isotherms. *Process Saf. Environ. Prot.* **2017**, *109*, 465–477. https://doi.org/10.1016/j.psep.2017.04.022.
35. Su, Z.; Ning, S.; Li, Z.; Zhang, S. High-efficiency separation of palladium from nitric acid solution using a silica-polymer-based adsorbent isoPentyl-BTBP/SiO2-P. *J. Environ. Chem. Eng*. **2022**, *10*, 107928. https://doi.org/10.1016/j.jece.2022.107928.
36. Wang, W.; Zhang, S.; Chen, L.; Li, Z.; Wu, K.; Zhang, Y.; Su, Z.; Yin, X.; Hamza, M.F.; Wei, Y.; et al. Efficient separation of palladium from nitric acid solution by a novel silica-based ion exchanger with ultrahigh adsorption selectivity. *Sep. Purif. Technol.* **2023**, *322*, 124326. https://doi.org/10.1016/j.seppur.2023.124326.
37. Adimule, V.; Nandi, S.S.; Yallur, B.C.; Bhowmik, D.; Jagadeesha, A.H. Optical, Structural and Photoluminescence Properties of Gd_x SrO: CdO Nanostructures Synthesized by Co Precipitation Method. *J. Fluoresc.* **2021**, *31*, 487–499. https://doi.org/10.1007/s10895-021-02683-7.
38. Zhang, Z.; Gu, P.; Zhang, M.; Yan, S.; Dong, L.; Zhang, G. Synthesis of a robust layered metal sulfide for rapid and effective removal of Sr^{2+} from aqueous solutions. *Chem. Eng. J.* **2019**, *372*, 1205–1215. https://doi.org/10.1016/j.cej.2019.04.193.
39. Gupta, K.; Yuan, B.; Chen, C.; Varnakavi, N.; Fu, M.-L. $K_{2x}Mn_xSn_{3-x}S_6$ (x = 0.5–0.95) (KMS-1) immobilized on the reduced graphene oxide as KMS-1/r-GO aerogel to effectively remove Cs^+ and Sr^{2+} from aqueous solution. *Chem. Eng. J.* **2019**, *369*, 803–812. https://doi.org/10.1016/j.cej.2019.03.109.
40. Yin, L.; Kong, X.; Shao, X.; Ji, Y. Synthesis of DtBuCH18C6-coated magnetic metal–organic framework Fe3O4@UiO-66-NH2 for strontium adsorption. *J. Environ. Chem. Eng.* **2019**, *7*, 103073. https://doi.org/10.1016/j.jece.2019.103073.
41. Ma, J.; Zhang, Y.; Ouyang, J.; Wu, X.; Luo, J.; Liu, S.; Gong, X. A facile preparation of dicyclohexano-18-crown-6 ether impregnated titanate nanotubes for strontium removal from acidic solution. *Solid State Sci.* **2019**, *90*, 49–55. https://doi.org/10.1016/j.solidstatesciences.2019.02.002.
42. Kudo, T.; Ito, T.; Kim, S.-Y. Adsorption behavior of Sr (II) from high-level liquid waste using crown ether with ionic liquid impregnated silica adsorbent. *Energy Procedia* **2017**, *131*, 189–194. https://doi.org/10.1016/j.egypro.2017.09.426.
43. Zhang, A.; Xiao, C.; Liu, Y.; Hu, Q.; Chen, C.; Kuraoka, E. Preparation of macroporous silica-based crown ether materials for strontium separation. *J. Porous Mater.* **2010**, *17*, 153–161. https://doi.org/10.1007/s10934-009-9287-2.